Room Temperature Buried Molecular Engineering Boosts the Photovoltaic Performance of Wide-Bandgap and All-Perovskite Tandems

Shaopeng Liao[1,2#], Guang Li[3#], Mengqi Ren[1], Ying Peng[1], Weitao Zhao[1], Zichao Xu[1], Hongsen Cui[3], Chen Tao[1], Haibing Wang[1], Chen Wang[1], Fang Yao[1], Xiaojuan Cao[1], Jiwei Liang[1], Mingming Hu[1], Yansong Ge[1], Xuzhi Hu[1]*, Jian Wen[1,2]*, Weijun Ke[3]*, Guojia Fang[1,3]*

[1] School of Electronics and Electrical Engineering, and State Key Laboratory of New Textile Materials and Advanced Processing, Wuhan Textile University, Wuhan, Hubei 430200, People's Republic of China

[2] College of Physics and Electronic Science, Hubei Key Laboratory of Photoelectronic Conversion Materials and Devices, School of Materials Science and Engineering, Hubei Normal University, Huangshi, Hubei 435002, People's Republic of China

[3] School of Physics and Technology, Wuhan University, Wuhan 430072, People's Republic of China.

S.P. Liao. and G. Li. contributed equally to this work.

* Corresponding author: Xuzhi Hu, xzhu@wtu.edu.cn;

Guojia Fang, gjfang@whu.edu.cn;

Jian Wen, jwenhb@hbnu.edu.cn;

Weijun Ke, weijun.ke@whu.edu.cn

Experimental section

Materials

4PADCB (4-(7H-dibenzo[c,g]carbazol-7-yl)butyl)phosphonic acid) were purchased from TCI. $Pb(SCN)_2$ (lead thiocyanate), SnF_2 (tin fluoride) and CsI (cesium iodide) were purchased from Sigma-Aldrich. NiO_X (Nickel oxide nanocrystals), MAI (methylammonium iodide), MACl (methylammonium chloride), PEAI (Phenethylamine hydroiodide), PbI_2 (lead iodide), $PbBr_2$ (lead bromide), FAI (formamidinium iodide) and SnI_2(tin iodide) was purchased from Youxuan New Energy Technology. GBAM（4-Guanidinobenzoic Acid Methanesulfonate）and Ethanol (Anhydrous) was purchased from Macklin. Fullerene (C_{60}), bathocuproine (BCP) and $EDAI_2$ (ethylenediammonium diiodide), PDADI (1,3-Diaminopropane dihydrochloride) was purchased from Xi'an polymer light technology. DMF (N, N-dimethyl formamide), IPA (isopropanol), CB(chlorobenzene), and DMSO (dmethyl sulfoxide) were acquired from Sigma-Aldrich. PEDOT: PSS (Clevios PVP Al4083) was purchased from Heraeus.

Device fabrication

Fabrication of 1.78eV WBG PSCs

The precursor solution for perovskite film deposition was prepared by mixing FAI, CsI, $PbBr_2$, and PbI_2 in a mixture of DMF and DMSO at a concentration of 1.2 M. The molar ratios of FA^+/Cs^+ and I^-/Br^- were maintained at 8:2 and 6:4, respectively. Additionally, a 1 mol% concentration of $Pb(SCN)_2$ was included, which was found to improve device performance.The precursor solution was stirred at room temperature for 12 hours. The ITO (Indium tin oxide) glass substrate was cleaned by sequentially washing it with detergent, deionized water, acetone, and ethanol. The substrate was dried with N_2 and further cleaned with ultraviolet ozone for 15 mins(minutes). After ultraviolet ozone treatment for 15 mins, the substrates were then spin-coated with NiO_X (10 mg/mL in deionized water) nanoparticle dispersion. NiO_X solution was spin-coated onto the ITO substrate at 3,000 rpm for 30 s and heated at 130 ℃ for 30 mins. Then, the films were transferred to a nitrogen-filled glovebox and 4PADCB (0.5 mg/mL in ethanol) was

spin-coated on the substrates at 3,000 rpm for 30 s and heated at 100 ℃ for 10 mins. GBAM (2mg/mL in ethanol) was spin-coated on the substrates at 4,000 rpm for 30s and dried in nitrogen-filled glovebox for 60 mins. The perovskite film was deposited on the substrate using a two-step spin-coating procedure. The first step involved spinning at 2,000 rpm for 10 seconds with an acceleration of 200 rpm s^{-1}. The second step involved spinning at 6,000 rpm for 50 seconds with an acceleration of 2,000 rpm s^{-1}. During the second spin-coating step, 350 μl of diethyl ether was dropped onto the spinning substrate at 30 seconds before the end of the procedure. The substrates were then transferred to a hotplate and heated with a two-step procedure: 60 °C for 2 minutes, followed by 100 °C for 10 minutes. After cooling to room temperature, a solution of PDADI in IPA (isopropyl alcohol) (2 mg ml^{-1}) was dropped onto the perovskite film and spin-coated at 4,000 rpm for 30 seconds. The substrate was then annealed at 100 °C for 10 minutes. Subsequently, the electron transport layers (ETLs) C_{60} (20 nm), BCP (7 nm), and the metal electrode Cu (100 nm) were evaporated onto the substrate using a high-vacuum thermal evaporator. The active area of the devices was defined using a shadow mask.

Fabrication of 1.25eV NBG PSCs

The cleaning of ITO substrates is the same as the above process in 1.78eV PSCs. Next, PEDOT: PSS solutions were spin-coated on the substrates at 5000 rpm for 30 s and annealed at 140°C for 30 min. After annealing, the substrates were immediately transferred into an N_2-filled glovebox. The perovskite precursors after filtering were directly deposited on the substrates by a one-step spin-coating method at 1000 rpm for 10 s and 4000 rpm for 40 s. 400 μL of CB was dropped on the films at the 20th second before the end of spin-coating. The substrates with perovskite films were annealed at 100℃ for 10 min. In the following, the $EDAI_2$ (1mg mL^{-1} in IPA) solution was spin-coated onto the perovskite films at 4000 rpm for 30 s, and the films were annealed at 100 ℃ for 7 min. Finally, C_{60} (20 nm), BCP (7 nm), and Cu (100 nm) were thermally evaporated under a high vacuum chamber (1×10^{-4} Pa) to complete the devices.

Fabrication of 1.53eV normal band gap PSCs

The cleaning of ITO substrates is the same as the above process in 1.78eV PSCs. ($FA_{0.85}MA_{0.1}Cs_{0.05}PbI_3$): 19.45 mg CsI, 23.85 mg MAI, 219.26 mg FAI and 746.83 mg PbI_2 were added in 1 mL mixed DMF and DMSO solution (820 μL DMF + 180 μL DMSO), 15 mol% MACl was added to improve the quality of perovskite films. The cleaned Glass/ITO substrates were treated with UV ozone for 15 min before use. After that, 100 μL 4PADCB (0.8 mg mL^{-1} in ethanol) solution was spun cast onto the substrates at 3000 rpm for 30 s and annealed at 100 ℃ for 10 min in glove box. Then, 100μL GBAM (3.0 mg mL^{-1} in ethanol) solution was spun cast onto the substrates at 3000 rpm for 30 s and annealed at 100 ℃ for 5 min. For the normal-bandgap perovskite, 35 μL perovskite solution was spun cast at 1000 rpm for 10 s with an acceleration of 500 rpm/s and 5000 rpm for 40 s with an acceleration of 1000 rpm/s. 400 μL of DE was dripped onto the center of the films at the 7 s before the end of the procedure. The perovskite films were annealed at 120 ℃ for 10 min. Then, 100 μL $EDAI_2$&PEAI (0.5&1.5 mg mL^{-1} in IPA) mixed solution was spin-coated on the as-prepared perovskite substrates at 5000 rpm for 25 s and annealed at 100 ℃ for 5 min. The samples were then transferred to an evaporator. C_{60} (20 nm), BCP (7 nm) and Cu (100 nm) were thermally deposited sequentially to complete the devices.

Fabrication of 2-T tandem PSCs

For the 2-T tandem PSCs, a 20 nm layer of atomic layer deposition (ALD) SnO_X was utilized instead of BCP (bathocuproine). A thin layer of 1 nm Au was deposited by thermal evaporation under a high vacuum chamber (1×10^{-4} Pa). Next, PEDOT: PSS solutions were spin-coated on the substrates at 5000 rpm for 30 s and annealed at 100°C for 30 min. After annealing, the substrates were immediately transferred into an N_2-filled glovebox for the fabrication of the NBG subcell as mentioned above.

Characterization and analysis

Film characterizations

PLQY measurements were characterized by a system with an integrating sphere and an

excitation wavelength of 365 nm. The fixed light intensity of 100 mW $cm^{-2}$was used for the PLQY measurements. The contact angle of perovskite precursor on different substrates (Glass/ITO/NiO_X/4PADCB or Glass/ITO/NiO_X/GBAM/4PADCB) was determined using a SL200KB dynamic contact angle analyzer. The perovskite bottom interface was characterized with XPS, SEM, KPFM, PL Mapping and the thin film preparation procedure was shown in Figure S3. XPS measurements were conducted with a monochromatic Al-Kα x-ray source by an XPS/UPS system (AXIS SUPRA+). XPS spectra were fitted using a Thermo Advantage software. Preceding the fitting process, energy levels were meticulously calibrated, with the reference C1s level set at 284.8 eV. The morphology of the films was observed using scanning electron microscopy (SEM) with a JSM-7800 microscope operating at an accelerating voltage of 5 kV. AFM and KPFM images were observed by a Bruker Dimension Icon XR equipment in a Scanasyst-Air and Peak force KPFM Mode. PL mapping was captured by a confocal laser scanning fluorescence microscopy (CLSM) (TCS SP8, Leica). A 552 nm laser was applied as the PL excitation source to detect and collect the PL signals at 650–750 nm. The crystal structures and phases of the perovskite films deposited on different substrates (Glass/ITO/NiO_X/4PADCB for control samples and Glass/ITO/NiO_X/GBAM/4PADCB for target samples) were characterized using an X-ray diffraction (XRD) instrument, specifically the Empyrean with a scan speed of 5 degree min^{-1}. UPS spectra were conducted in the Thermo Scientific Escalab 250Xi XPS/UPS system with a He I UV source at a bias voltage of -6 V. The absorption spectra of the films were measured using a Shimadzu UV-vis spectrophotometer, specifically the miniUV-1208 model. Surface roughness of the films was characterized with a Bruker Dimension Icon XR AFM.

Device characterizations

First, primitive *J-V* curves were obtained using a Keithley 2400 source meter under standard AM 1.5 G illumination (100mW cm^{-2}) produced by a solar simulator (Enlitech, SS-F5-3A), and the original J_{SC} is derived from the curve. The solar simulator

was calibrated to a 100mW cm^{-2} light intensity by a National Renewable Energy Laboratory-certified and KG3-filtered crystalline silicon solar cell. This sample is then placed in the EQE test system (Enli Technology Co. Ltd.), resulting in an integral J_{EQE}. The original J_{SC} is then calibrated by a coefficient based on the J_{EQE} obtained by the integral, so as to match the integral J_{EQE} measured by the EQE test (error range less than 2%). Current-voltage (*J-V*) curves and steady-state power outputs of the perovskite solar cells (PSCs) were measured under air mass 1.5 global (AM 1.5 G) conditions, with the measurements performed by Enli Technology Co. Ltd in a nitrogen atmosphere. A metal mask was used to mask the active area during the measurements, with a hole area being 0.070225 cm^2. The *J-V* measurements were carried out with a scan rate of 20 mV/s, covering a voltage range from 1.36 V to -0.1 V and then reversed back from -0.1 V to 1.36 V (-0.1V to 2.2V for 2-T tandem), with a dwell time of 50 ms at each voltage point. Space charge limited current (SCLC) curves of single-carrier devices were recorded using a Keithley 2400 source meter in the dark. Mott-Schottky curves with capacitance-voltage measurements were performed using a CHI760E electrochemical workstation from Shanghai Chenhua Instruments at 1 kHz. The bias voltages ranged from 1.5 V to 0 V, and an AC voltage of 20 mV was used to measure the corresponding capacitance at the different bias voltages.

Supplementary Note 1: Calculation of V_{OC} non-radiative recombination loss

The relationship between the photoluminescence quantum yield (PLQY) and the quasi-Fermi level splitting (QFLS) in the perovskite film can be described by the following equation, assuming that all photoluminescence (PL) emission originates from radiative recombination of free charges:

$$QFLS = QFLS_{rad} + K_B T ln(PLQY) \#(1)$$

In Equation (1), $QFLS_{rad}$ represents the $QFLS$ for the perovskite layer when only radiative recombination occurs. K_B is the Boltzmann constant, T is the temperature, and-$K_B T ln(PLQY)$ represents the QFLS loss due to non-radiative recombination.

Additionally, the non-radiative recombination loss (ΔV_{OC}) in the V_{OC} can be calculated

using the following equation:

$$\Delta V_{OC} = \frac{QFLS_{rad} - QFLS}{q} = - \frac{K_B T ln(PLQY)}{q} \#(2)$$

Supplementary Note 2: Cyclic voltammetry for surface density characterization

Cyclic voltammetry (CV) serves as a powerful electrochemical technique for quantifying the surface density of functional materials on electrode interfaces. By applying a controlled potential sweep between pre-defined limits, CV monitors the Faradaic current associated with redox-active species adsorbed or deposited on the electrode surface. The resulting current response correlates directly with the surface-confined electrochemical active sites, enabling precise determination of surface coverage through quantitative analysis of peak currents and integration of charge densities. Specifically, in the characterization of the molecular surface coverage, CV measurements were performed using a VIIUM electrochemical workstation in a three-electrode configuration at room temperature. Working electrodes were prepared via spin-coating onto an ITO-coated glass substrate, with an exposed electrode area of 20 mm×15 mm (3 cm^2). A platinum plate and an Ag/AgCl electrode (immersed in a 3.0 M KCl solution) served as the counter and reference electrodes, respectively. Experiments were conducted in an Ar-saturated solution of 1,2 dichlorobenzene (o-DCB) with 0.1 M tetrabutylammonium hexafluorophosphate (TBA^+PF6^-) as the supporting electrolyte, ensuring an inert and conductive environment. All potentials were referenced against the ferrocene/ferrocenium (Fc/Fc+) redox couple, which acted as an internal standard. The effective surface coverage (Γ^*) of 4PADCB or 4PADCB/GBAM on NiO_X surface was measured by the slope of a linear dependency of the oxidative peak intensity against the scan rate as follows:

$$i_{p,o} = \frac{n^2F^2}{4RTN_A} A\Gamma^* v$$

here, $i_{p,o}$ denotes the oxidative peak current, n is the number of electrons transferred, F stands for the Faraday constant (96485.33 $C \cdot mol^{-1}$), R is the universal gas constant (8.314 $J \cdot K^{-1}mol^{-1}$), T denotes the temperature, N_A is the Avogadro constant (6.022×1023 mol^{-1}), A represents the electrode area, and v represents the scan rate of the voltage.

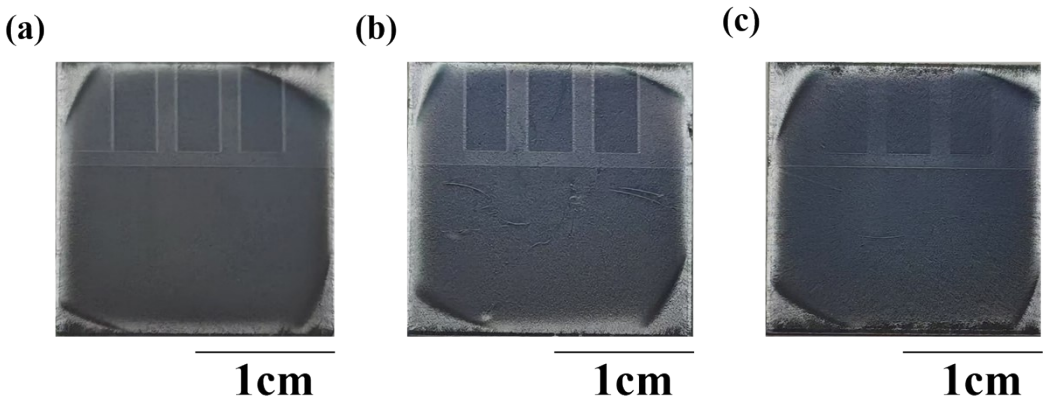

Figure S1. Optical photos of three different perovskite films deposited on (a) NiO_X/4PADCB, (b) GBAM film after annealing for 10 min and (c) GBAM film after drying for 1 h.

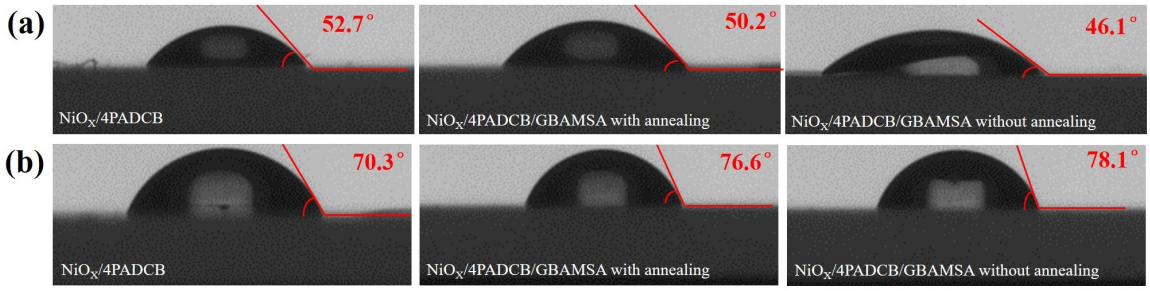

Figure S2. Contact angle measurements using (a) perovskite solution and (b) water as a test solvent, respectively. The text in the picture indicates the structures of different substrates.

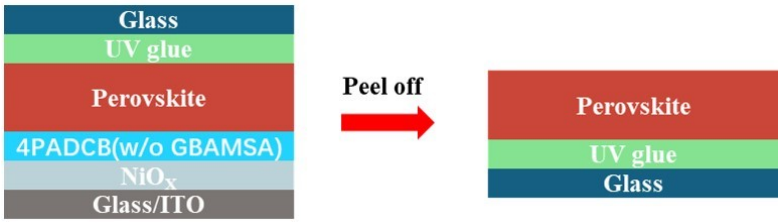

Figure S3. Schematic of peeling off perovskite films from ITO glass substrates with a Ultraviolet (UV) illumination encapsulation glue. The buried interfaces are used for various characterization.

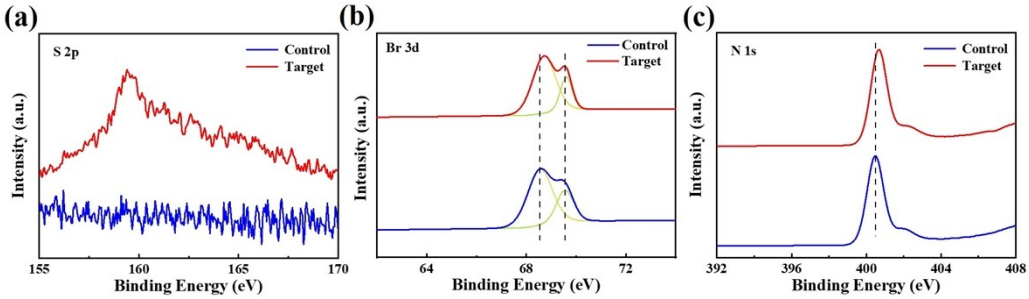

Figure S4. (a) S 2p (b) Br 3d and (c) N 1s XPS spectra for control and target perovskite films.

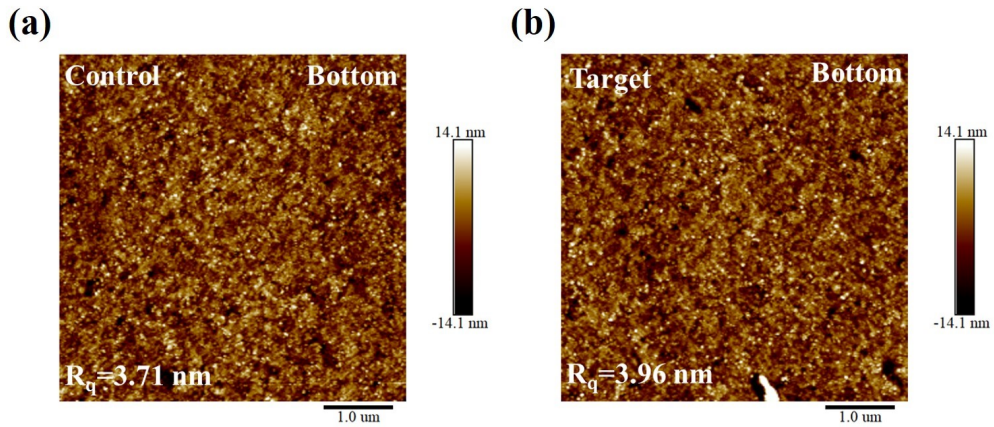

Figure S5. AFM images of the buried interface of the control and target perovskite film

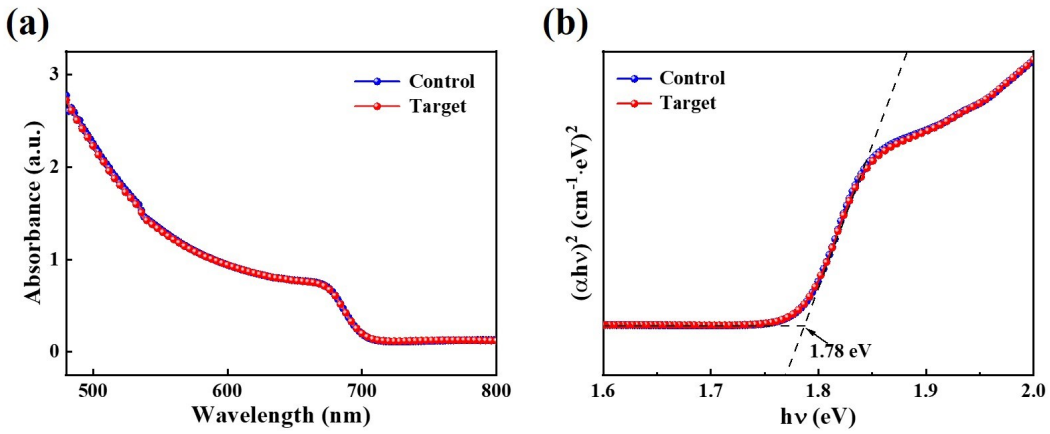

Figure S6. (a) UV–vis absorption spectra and (b) Tauc plots with the corresponding optical bandgaps of control and target perovskite films

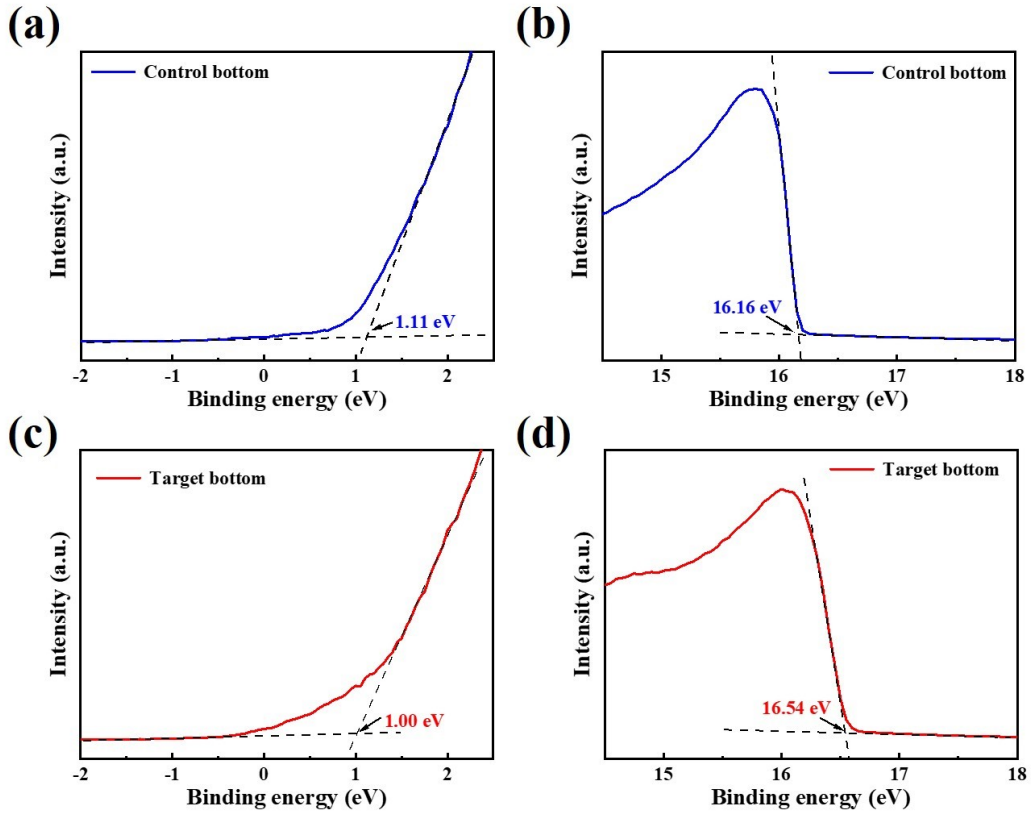

Figure S7. UPS spectra in the cutoff and the onset region for the perovskites (a), (b) without and (c), (d) with GBAM interface engineering treatment.

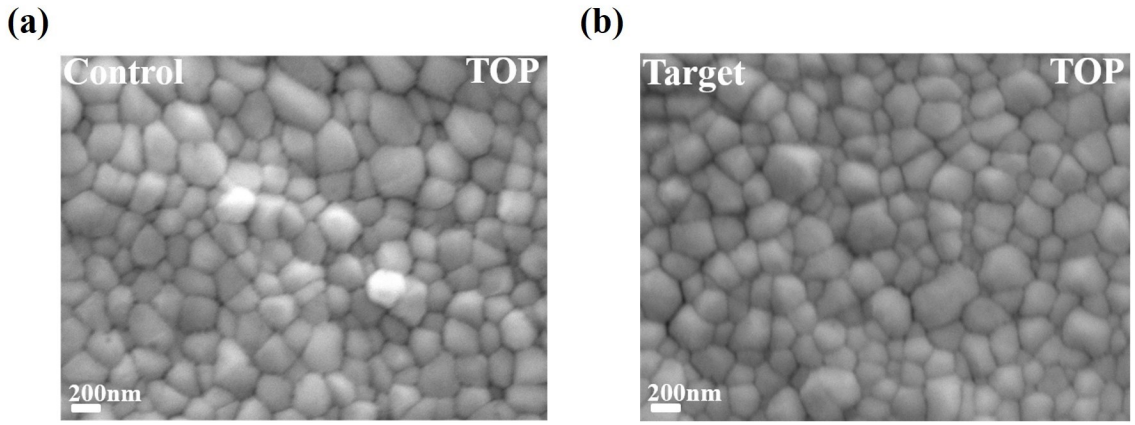

Figure S8. (a), (b) SEM images of the surfaces of the control, and target perovskite films.

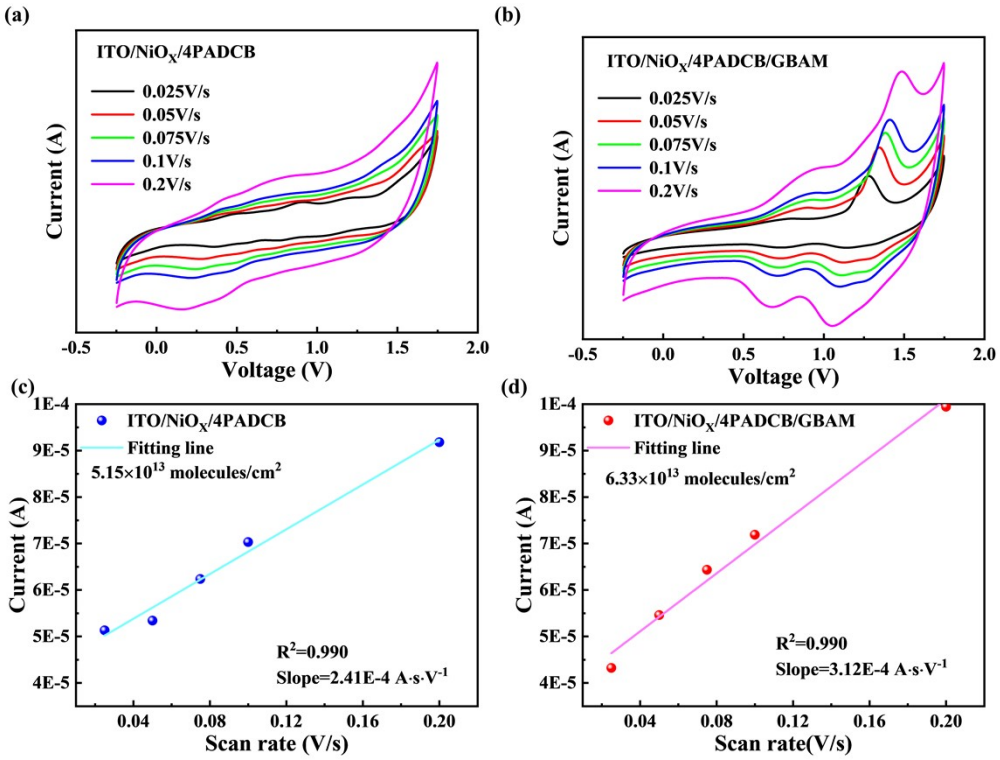

Figure S9. Cyclic voltammograms of (a) ITO/NiO_X/4PADCB and (b) ITO/NiO_X/4PADCB/GBAM as the working electrode measured in Ar-saturated o-DCB solution under different voltage scan rates. (c) The fitting linear relationship between peak current and scan rate derived from the oxidation peaks of NiO_X/4PADCB and NiO_X/4PADCB/GBAM in cyclic voltammetry.

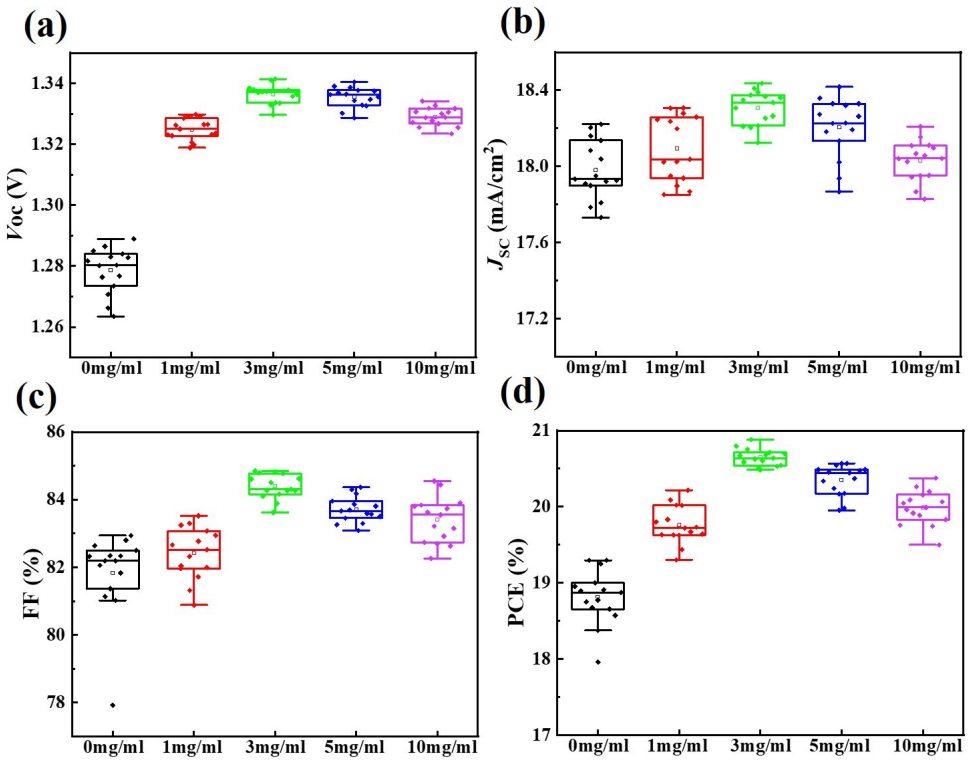

Figure S10. Statistical results of V_{OC} (a), J_{SC} (b), FF (c) and PCE (d) using different concentration of GBAM in ethanol.

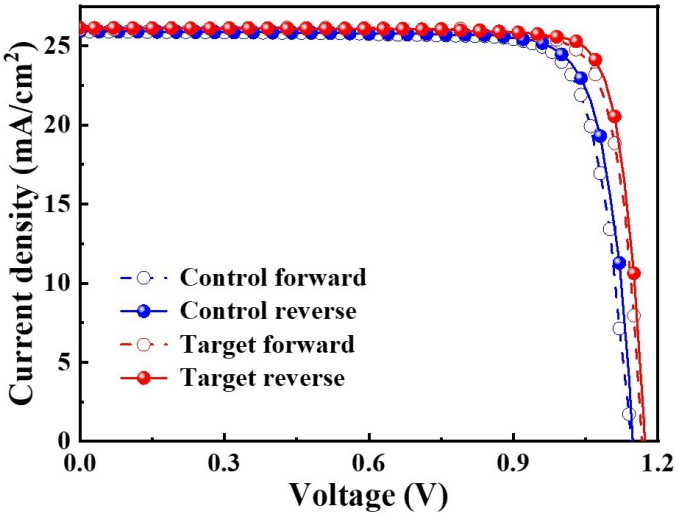

Figure S11. The champion *J-V* curves of 1.53 eV band gap control and target perovskite solar cells under forward and reverse scanning.

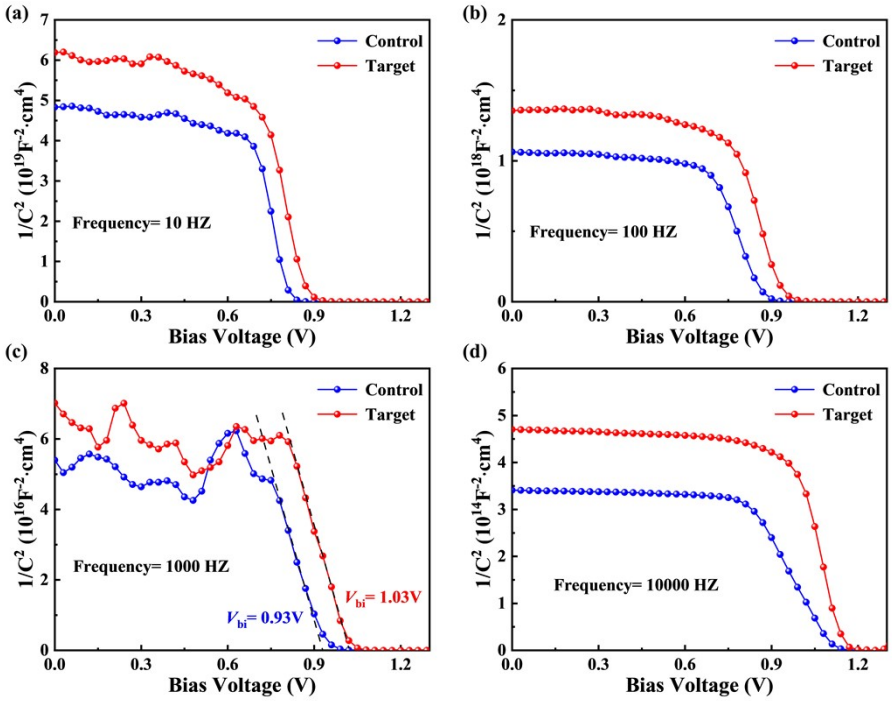

Figure S12. Mott-Schottky plots measured at different frequencies (10 Hz(a), 100 Hz(b), 1kHz(c) and 10 kHz(d)) for the control and target devices.

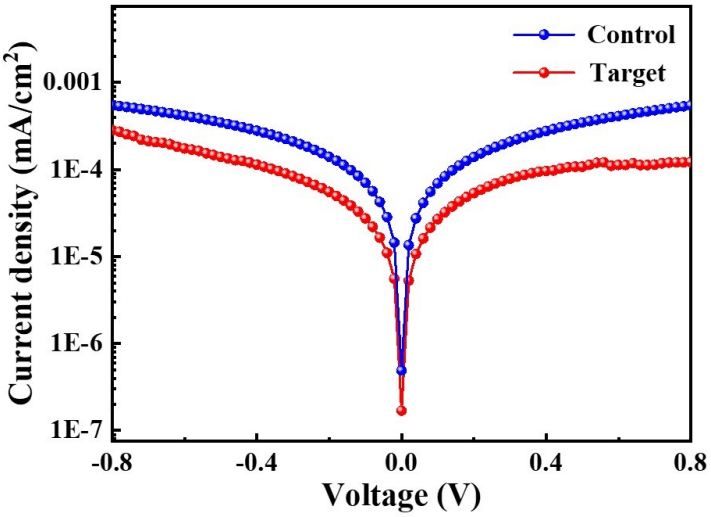

Figure S13. The dark current density-voltage (*J-V*) curves of the control and target devices.

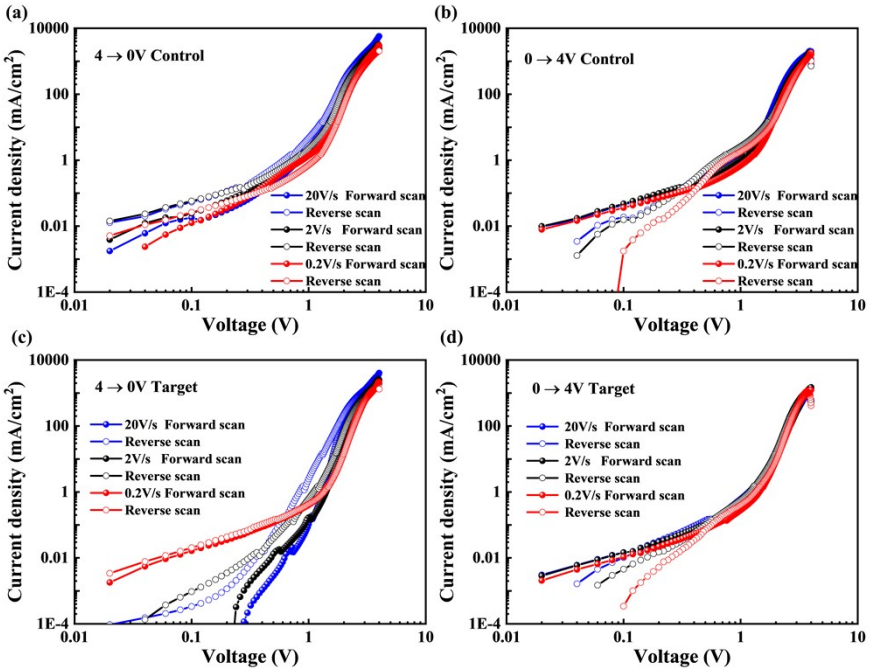

Figure S14. SCLC of the control and target perovskite device for varying scan speeds, starting conditions and sweep directions. (a)Voltage sweep from V_{max}= 4V to V_{min}= 0V of the control device. (b)Voltage sweep from V_{min}=0V to V_{max}=4V of the control device. (c)Voltage sweep from V_{max}= 4V to V_{min}= 0V of the target device. (d)Voltage sweep from V_{min}=0V to V_{max}=4V of the target device.

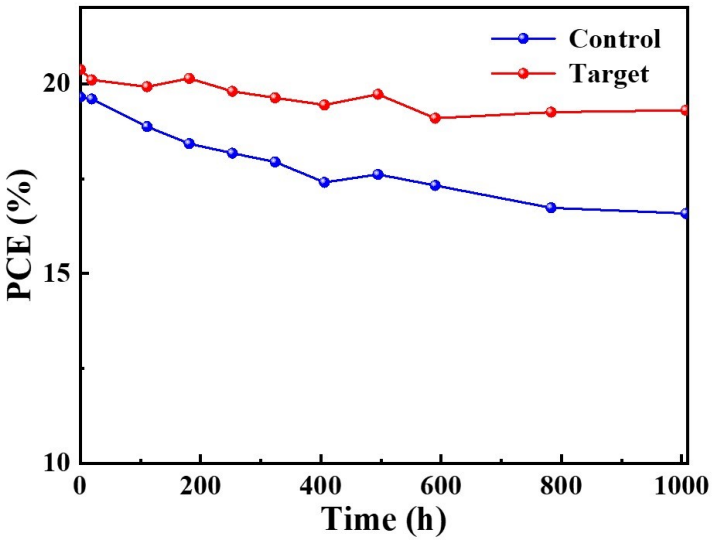

Figure S15. Storage stability measurement results of the control device and the target device in a glove box at 25 ± 5 °C with N_2 for 1000h.

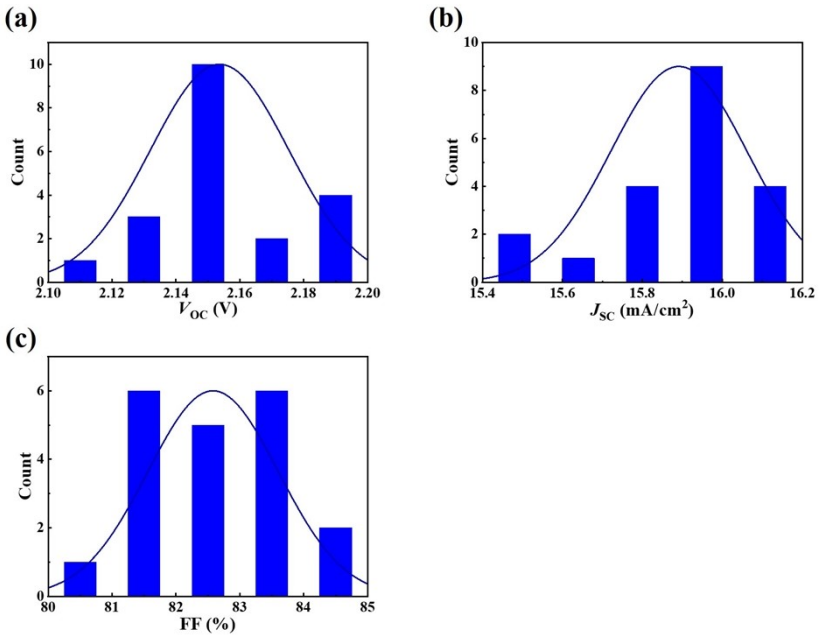

Figure S16. Distribution histograms of (a)V_{OC}, (b)J_{SC} and (c)FF for individual 20 tandem devices.

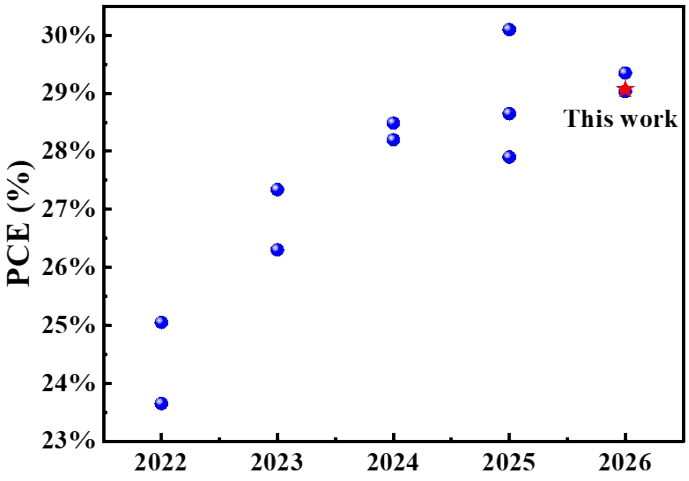

Figure S17. The power conversion efficiency (PCE) evolution of the 4-T all-perovskite tandem solar cells.

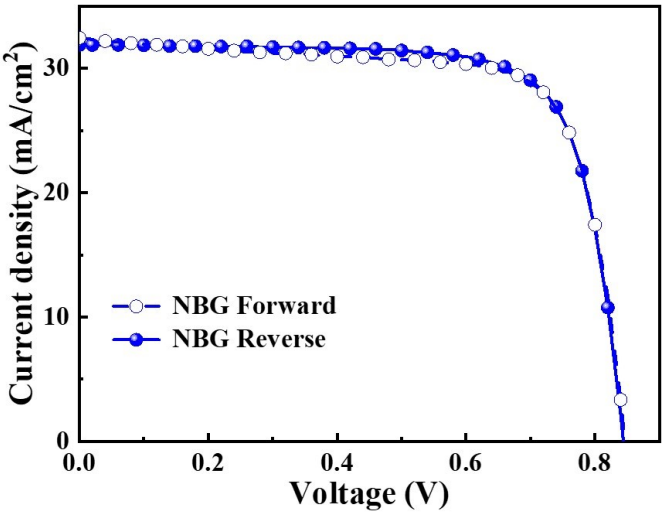

Figure S18. *J–V* characteristics of the champion NBG device under different scan directions.

Table S1. Carrier lifetimes obtained from TRPL spectra of perovskite films side with and without GBAM.

Sample	τ_1(ns)	τ_2(ns)	Average Lifetime(ns)
Control	10	60	48
Target	42	149	114

Table S2. Carrier lifetimes obtained from TRPL spectra of ITO side with and without GBAM.

Sample	τ_1(ns)	τ_2(ns)	Average Lifetime(ns)
Control	51	127	89
Target	9	57	45

Table S3. Performance parameters table of 1.53 eV bandgap control and target champion devices.

Sample	Direction	J_{SC} (mA · cm^{-2})	V_{OC} (V)	FF (%)	PCE (%)
Control	Forward	25.92	1.140	81.32	24.02
	Reverse	25.91	1.150	82.28	24.42
Target	Forward	26.05	1.170	83.91	25.50
	Reverse	26.14	1.173	85.35	26.16

Table S4. The series resistance (R_S) and recombination resistance (R_{rec}) obtained from electronic impedance spectroscopy (EIS) spectra of perovskite films with and without GBAM interface engineering treatment.

Sample	R_S (Ω)	R_{rec} (Ω)
Control	10.6	17858
Target	8.6	27207

Table S5. Summary of the state-of-the-art 2-T all-perovskite tandem solar cells.

Year	PCE	Ref
2022	23.65%	1
2022	25.05%	2
2023	26.30%	3
2023	27.34%	4
2024	28.20%	5
2024	28.49%	6
2025	27.9%	7
2025	28.65%	8
2025	30.10%	9
2026	29.03%	10
2026	29.35%	11
2026	29.07%	**This work**

Table S6. Photovoltaic performance of single-junction NBG device.

Direction	V_{OC} (V)	J_{SC} (mA/cm^2)	FF (%)	PCE (%)
Forward	0.86	32.84	75.00	21.27
Reverse	0.87	32.37	78.80	22.26

Reference

1. X. Zhou, H. Lai, T. Huang, C. Chen, Z. Xu, Y. Yang, S. Wu, X. Xiao, L. Chen, C. J. Brabec, Y. Mai and F. Guo, *ACS Energy Letters*, 2022, **8**, 502-512.
2. C. L. Wang, Y. Zhao, T. S. Ma, Y. D. An, R. He, J. W. Zhu, C. Chen, S. Q. Ren, F. Fu, D. W. Zhao and X. F. Li, *Nature Energy*, 2022, **7**, 744-753.
3. J. W. Zhu, Y. Luo, R. He, C. Chen, Y. Wang, J. C. Luo, Z. J. Yi, J. Thiesbrummel, C. L. Wang, F. L. Lang, H. G. Lai, Y. L. Xu, J. C. Wang, Z. H. Zhang, W. Q. Liang, G. Y. Cui, S. Q. Ren, X. Hao, H. Huang, Y. Wang, F. Yao, Q. Q. Lin, L. L. Wu, J. Q. Zhang, M. Stolterfoht, F. Fu and D. W. Zhao, *Nature Energy*, 2023, **8**, 714-724.
4. S. Zhou, S. Q. Fu, C. Wang, W. W. Meng, J. Zhou, Y. R. Zou, Q. X. Lin, L. S. Huang, W. J. Zhang, G. J. Zeng, D. X. Pu, H. L. Guan, C. Wang, K. L. Dong, H. S. Cui, S. X. Wang, T. Wang, G. J. Fang and W. J. Ke, *Nature*, 2023, **624**, 69-+.
5. Y. Q. Bao, J. Zeng, Y. T. Xu, G. S. Xie, H. Hu, X. Lei, D. Wang, J. Y. Zhang, W. B. Peng, Z. X. Liu, P. D. Zhu, G. P. Qu, L. B. Qiu, L. Yan, Y. Zhang, X. Z. Wang and B. M. Xu, *Adv Energy Mater*, 2025, **15**.
6. Y. Pan, J. Wang, Z. Sun, J. Zhang, Z. Zhou, C. Shi, S. Liu, F. Ren, R. Chen, Y. Cai, H. Sun, B. Liu, Z. Zhang, Z. Zhao, Z. Cai, X. Qin, Z. Zhao, Y. Ji, N. Li, W. Huang, Z. Liu and W. Chen, *Nat Commun*, 2024, **15**, 7335.
7. Q. He, P. Liu, H. Li, W. Feng, Y. Ma, M. Ma, M. Wu, Y. Yang, X. Lin, Z. Xiao, S. Wu, J. Fan and Y. Mai, *Adv Energy Mater*, 2025, **15**.
8. W. Li, G. Liu, X. Wen, X. Jiang, H. Wu, M. Ma, W. Zhou, H. Liang, Q. Zhou, Y. Liu, R. Xu, W. Wang, Z. Su, W. Zhou, X. Gao and Z. Ning, *Angew Chem Int Ed Engl*, 2025, **64**, e202511743.
9. R. Lin, H. Gao, J. Lou, J. Xu, M. Yin, P. Wu, C. Liu, Y. Guo, E. Wang, S. Yang, R. Liu, D. Zhou, C. Ding, A. D. Bui, N. Yin, D. H. Macdonald, C. Q. Ma, Q. Chen, K. Xiao, X. Luo, Y. Liu, L. Li, Y. Li, C. Chang and H. Tan, *Nature*, 2025, **648**, 600-606.
10. W. Li, G. Li, S. Zhou, Y. Gou, B. Jin, J. Yan, W. Dai, Y. Li, H. Zhang, W. Ke, T. Wang and H. Xu, *Adv Mater*, 2026, DOI: 10.1002/adma.202522942, e22942.
11. D. Wang, Z. Liu, Z.-W. Gao, X. Lei, P. Zhu, J. Zeng, Q. Li, L. Wang, Z. Zhang, M. Gu, S. He, Y. Bao, Q. Lian, J. Li, Z. Song, Y. Xu, D. Lei, X. Wang, A. K. Y. Jen and B. Xu, *Nature Energy*, 2026, DOI: 10.1038/s41560-026-01964-4.